# Hydrothermal Synthesis of Lithium and Sodium Manganese Oxides and Their Metal Ion Extraction/Insertion Reactions

Qi Feng,*,† Hirofumi Kanoh, Yoshitaka Miyai, and Kenta Ooi*

*Shikoku National Industrial Research Institute, 2217-14 Hayashi-cho Takamatsu-shi Kagawa 761-03, Japan*

*Received January 6, 1995. Revised Manuscript Received April 17, 1995*®

Spinel-type lithium manganese oxide (LMO) and birnessite-type sodium manganese oxide (NMO) were prepared by hydrothermal treatment of $\gamma$-$MnO_2$ with LiOH and NaOH solutions, respectively. The extraction/insertion reactions of the alkali-metal ions with the manganese oxides were investigated by chemical, X-ray, DTA-TG analyses, FT-IR spectroscopy, pH titration, and $K_d$ measurements. $Li^+$ and $Na^+$ were topotactically extracted from LMO and NMO, respectively, by two different mechanisms: redox-type and ion-exchange-type reactions. The pH titration studies indicated that the acid-treated LMO (LMO(H)) has a remarkably larger adsorptive capacity for $Li^+$ than those for the other alkali-metal ions. The acid-treated NMO (NMO(H)) showed tetrabasic acid behavior toward $Li^+$, but monobasic acid behavior toward the other alkali-metal ions. A new model was proposed for the insertion reaction of alkali-metal ions with NMO(H). LMO(H) and NMO(H) showed ion-sieve properties for the adsorption of alkali-metal ions. The $K_d$ measurements suggested that the effective pore radii of the ion sieves are about 0.7 Å for LMO(H) and 1.5 Å for NMO(H).

## Introduction

Manganese oxides show excellent properties for adsorption of metal ions.[1-9] The adsorptive properties are strongly dependent on the crystal structure of the manganese oxides. The manganese oxides with tunnel structures show ion-sieve properties for the adsorption of metal ions. Spinel-type manganese oxides with a three-dimensional (1 × 3) tunnel structure show a specific high selectivity for the adsorption of $Li^+$ among alkali-, and alkaline-earth, and transition-metal ions.[10-22] Hollandite- or cryptomelane-type manganese oxides with a one-dimensional (2 × 2) tunnel structure show a specific high selectivity for the adsorption of metal ions with an effective ionic radius of about 1.4 Å, e.g., $K^+$, $Rb^+$, and, $Ba^{2+}$.[9,23-26] The selective properties can be explained on the basis of the ion-sieve effect of the tunnels. The (1 × 3) tunnel of the spinel structure is suitable in size for fixing $Li^+$,[10-16] and the (2 × 2) tunnel of the hollandite structure is suitable in size for fixing metal ions with an effective ionic radius of about 1.4 Å.[23-26]

Manganese oxide with the tunnel structure can be obtained by topotactically extracting alkali- or alkaline-earth-metal ions from the manganese oxide containing the corresponding alkali- or alkaline-earth-metal ions using an acid treatment.[10-25,27] Our studies of the spinel-type or hollandite-type manganese oxides indicated that the metal ion extraction/insertion reactions progress by two types of reactions.[18-22,26] One is a redox-type, and the other is an ion-exchange-type. The proportions of the redox-type and ion-exchange-type reactions are dependent on the preparation conditions of the manganese oxides, due to the easy change of the manganese oxidation state.[19-22,26]

The hydrothermal method seems to be promising for the synthesis of metal oxides which are difficult to obtain by solid-state reaction, especially for the low-temperature stable phases. This is because the hydrothermal reaction can be carried out at a low tempera-

† Present address: Research Laboratory of Hydrothermal Chemistry, Faculty of science, Kochi University, 2-5-1 Akebono-cho Kochi-shi 780, Japan

® Abstract published in *Advance ACS Abstracts,* May 15, 1995.

(1) Vesely, V.; Pekarek, V. *Talanta* **1972**, *19*, 1561.
(2) Murray, D. J.; Healy, T. W.; Fuerstenau, D. W. *Adv. Chem. Ser.* **1968**, *79*, 74.
(3) Murray, J. W. *Geochim. Cosmochim. Acta* **1975**, *39*, 505.
(4) Loganathan, P.; Burau, R. G. *Geochim. Cosmochim. Acta* **1973**, *37*, 1277.
(5) Gadde, R. R.; Laitinen, H. A. *Anal. Chem.* **1974**, *46*, 2022.
(6) Gerevini, T.; Somigliana, R. *Energ. Nucl.* **1959**, *6*, 339.
(7) Singh, O. V.; Tandon, S. N. *Int. J. Appl. Radiat. Isotopes* **1977**, *28*, 701.
(8) Bystrom, A.; Bystrom, A. M. *Acta Crystallogr.* **1950**, *3*, 146.
(9) Tsuji, M.; Komarneni, S.; Tamaura, Y.; Abe, M. *Mater. Res. Bull.* **1992**, *27*, 741.
(10) Ooi, K.; Miyai, Y.; Katoh, S. *Sep. Sci. Technol.* **1987**, *22*, 1779.
(11) Shen, X. M.; Clearfield, A. *J. Solid State Chem.* **1986**, *64*, 270.
(12) Vol'khin, V. V.; Leont'eva, G. V.; Onolin, S. A. *Neorg. Mater.* **1973**, *6*, 1041.
(13) Leont'eva, G. V.; Chirkova, L. G. *Zh. Prikl. Khin.* **1988**, *61*, 734.
(14) Ooi, K.; Miyai, Y.; Katoh, S. *Sep. Sci. Technol.* **1986**, *21*, 755.
(15) Ooi, K.; Miyai, Y.; Katoh, S. *Solvent Extr. Ion Exch.* **1987**, *5*, 561.
(16) Ooi, K.; Miyai, Y.; Katoh, S.; Maeda, H.; Abe, M. *Bull. Chem. Soc. Jpn.* **1988**, *61*, 407.
(17) Miyai, Y.; Ooi, K.; Katoh, S. *J. Colloid Interface Sci.* **1989**, *130*, 5251.
(18) Ooi, K.; Miyai, Y.; Katoh, S.; Maeda, H.; Abe, M. *Langmuir* **1989**, *5*, 150.
(19) Ooi, K.; Miyai, Y.; Sakakihara, J. *Langmuir* **1991**, *7*, 1167.
(20) Feng, Q.; Miyai, Y.; Kanoh, H.; Ooi, K. *Langmuir* **1992**, *8*, 1861.
(21) Feng, Q.; Miyai, Y.; Kanoh, H.; Ooi, K. *Chem. Mater.* **1993**, *5*, 311.
(22) Liu, Y. F.; Feng, Q.; Ooi, K. *J. Colloid Interface Sci.* **1994**, *163*, 130.
(23) Tsuji, M.; Abe, M. *Solv. Extr. Ion Exch.* **1984**, *2*, 253.
(24) Tsuji, M.; Abe, M. *Bull. Chem. Soc. Jpn.* **1985**, *58*, 1109.
(25) Tsuji, M.; Komarneni, S. *J. Mater. Res.* **1993**, *8*, 611.
(26) Feng, Q.; Miyai, Y.; Kanoh, H.; Ooi, K. *Chem. Mater.* **1995**, *7*, 148.
(27) Hunter, J. C. *J. Solid State Chem.* **1981**, *39*, 142.

0897-4756/95/2807-1226$09.00/0 

ture, while under high pressure in the aqueous solution. The hydrothermal synthesis of manganese oxides has been reported by several authors. The manganese oxides with layered structures have been obtained under hydrothermal conditions.[28–31] However, the metal-ion-adsorptive properties for these manganese oxides have not yet been clarified.

The present paper describes a hydrothermal synthesis of lithium and sodium manganese oxides and a fundamental study of extraction/insertion reactions of the alkali-metal ions with the oxides in the aqueous phase.

## Experimental Section

**Sample Preparation.** Lithium and sodium manganese oxides were prepared by hydrothermal treatment of $\gamma$-$MnO_2$ (electrolytic manganese dioxide no. 1) with LiOH and NaOH solutions, respectively. Manganese dioxide (10 g) and 100 mL of 0.5 M LiOH or 4 M NaOH solution were placed in a Teflon-lined, sealed, stainless steel vessel (110 mL) and autoclaved at 170 °C under autogenous pressure. The vessel was cooled to room temperature, and the suspension was filtered, washed with water, and air-dried at room temperature for 3 days. The lithium and sodium manganese oxides which were obtained by the hydrothermal treatment over 24 days were designated as LMO and NMO, respectively.

Samples of LMO and NMO were immersed in a 1 M nitric acid solution at room temperature for 2 days to obtain the acid-treated samples (LMO(H) and NMO(H)). The samples were filtered, washed with water, and air-dried at room temperature for 3 days.

**Chemical Analyses.** The available oxygen of each sample was determined by the standard oxalic acid method as described previously.[20] The mean oxidation number ($Z_{Mn}$) of manganese was evaluated from the value of available oxygen. The lithium, sodium, and manganese contents were determined after dissolving the sample in a mixed solution of $H_2SO_4$ and $H_2O_2$. Lithium and sodium concentrations were determined by atomic absorption spectrometry. Manganese concentration was determined by absorption spectrometry at 523 nm after oxidizing Mn to Mn(VII) with $(NH_4)_2S_2O_8$.

**Physical Analyses.** An X-ray analysis was carried out using a Rigaku type RINT1200 X-ray diffractometer with a graphite monochromator. Any mechanical deviation of diffraction angles was corrected by scanning the whole angle range with silicon powder. Infrared spectra were obtained by the KBr method on a JEOL infrared spectrometer Model JTR-RFX3001. DTA-TG curves were obtained on a MAC Science thermal analyzer (System 001, TG-DTA 2000) at a heating rate of 10 °C/min. The water content of the samples was calculated from the weight loss of the TG curve in a temperature range from 30 to 300 °C.

**pH Titration.** A 0.1-g portion of each acid-treated sample was immersed in a mixed solution (10 mL) of MCl + MOH (M = Li, Na, K, Cs) in varying ratios with intermittent shaking at 25 °C. The concentration of MCl was adjusted to 0.1 M. After the sample was shaken for 7 days, the pH of the supernatant solution was determined with a Horiba Model M8s pH meter.

**Distribution Coefficient ($K_d$).** $K_d$ values of alkali-metal ions were determined by the batch method. The acid-treated sample (0.1 g) was immersed in 10 mL of a solution containing $10^{-3}$ M each of $Li^+$, $Na^+$, $K^+$, $Rb^+$, and $Cs^+$ at pH 2. After attaining equilibrium (over 14 days), the metal ion concentrations in the solution were determined by atomic absorption spectrometry. The metal ion uptake was calculated from the concentration relative to the initial concentration in the solution. The $K_d$ value was calculated using the following equation:

$$K_d\ (\text{mL/g}) = \frac{\text{metal ion uptake (mmol/g of sample)}}{\text{metal ion concentration (mmol/mL solution)}}$$

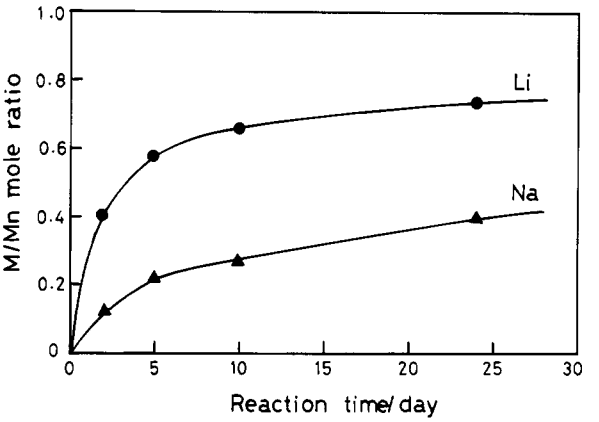


**Figure 1.** Dependence of lithium (●) and sodium (▲) contents on the time of hydrothermal treatment of the manganese oxide with LiOH and NaOH at 170 °C.

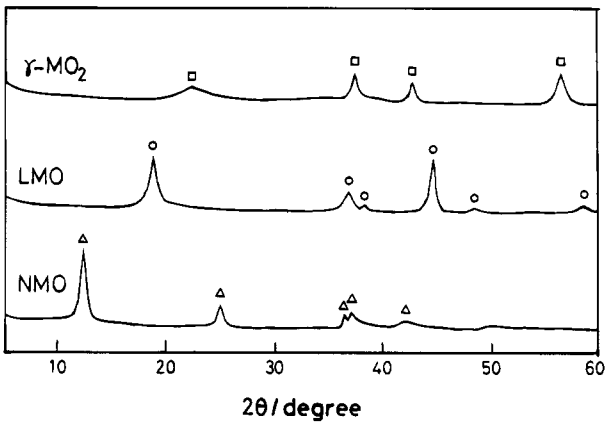


**Figure 2.** X-ray diffraction patterns of starting manganese oxide ($\gamma$-$MnO_2$), lithium manganese oxide (LMO), and sodium manganese oxide (NMO) prepared by hydrothermal treatment. □, peaks corresponding to $\gamma$-$MnO_2$ phase; ○, peaks corresponding to spinel phase; △, peaks corresponding to birnessite phase.

## Results and Discussion

**Preparation and Characterization of Lithium and Sodium Manganese Oxides.** Lithium and sodium content (Li/Mn and Na/Mn mole ratios) of the manganese oxides during the course of hydrothermal treatment at 170 °C are shown in Figure 1. Both the Li/Mn and Na/Mn mole ratios increase rapidly in the first 10 days; the rates of the increase of the Li/Mn and Na/Mn mole ratios become slower after 10 days. This tendency is more significant for the Li/Mn mole ratio than for the Na/Mn mole ratio. Since $Li^+$ has a smaller ionic radius, it can penetrate into the starting manganese oxide more easily, and it thus has a higher reactivity with the manganese oxide.

X-ray diffraction patterns of the lithium and sodium manganese oxides (LMO, NMO) obtained by hydrothermal treatment after 24 days are shown in Figure 2. The X-ray diffraction data indicate that LMO has a spinel structure (face-centered cubic system) with a lattice constant ($a_0$) of 8.18 Å. A monoclinic phase ($Li_2MnO_3$) was formed under the condition of high LiOH concen-

(28) Hirano, S.; Narita, R.; Naka, S. *Mater. Res. Bull.* **1984**, *19*, 1229.
(29) Morales, J.; Navas, J. J.; Tirado, J. L. *Solid State Ionics* **1990**, *44*, 125.
(30) Endo, T.; Kume, S.; Shimada, M.; Koizumi, M. *Mineral. Mag.* **1974**, *39*, 559.
(31) Strobel, P.; Durr, J.; Tuilier, M. H.; Charenton, J. C. *J. Mater. Chem.* **1993**, *3*, 453.

tration (>1 M). In the spinel structure, Mn ions can be distributed to 16d octahedral sites and $Li^+$ ions to 8a tetrahedral sites and Mn vacancies in 16d octahedral sites.[20,32,33] NMO has a birnessite (layered) structure with an interlayer distance of 7.19 Å along the *c* axis. The birnessite structure contains two-dimensional sheets of edge-shared $MnO_6$ octahedra, with sheets of water molecules and $Na^+$ ions between the sheets of edge-shared $MnO_6$ octahedra.[28,29,31,34,35]

The DTA-TG curves for sample LMO showed an endothermic peak around 120 °C with a weight loss (Figure 3a); this peak corresponds to the evaporation of adsorbed water. The DTA-TG curves for sample NMO showed endothermic peaks around 80, 120, and 450 °C with weight losses (Figure 3b). The peaks around 80 and 120 °C correspond to the evaporation of adsorbed water and the dehydration of the water of crystallization which locates between the sheets of $MnO_6$ octahedra. The peak around 450 °C can be ascribed to the transformation of Mn(IV) to Mn(III) with the release of oxygen gas.[36]

Chemical analysis results for samples of LMO, NMO, and starting manganese oxide are summarized in Table 1. Compositional formulas of LMO and NMO can be written as $Li_{1.27}Mn_{1.73}O_4 \cdot 0.4H_2O$ and $Na_{0.40}Mn_{2.15}O_2 \cdot 0.6H_2O$, respectively. The mean oxidation numbers ($Z_{Mn}$) of Mn are almost constant before and after the hydrothermal treatment, indicating that no redox reaction occurs.

**Characterization of Acid-Treated Samples.** When LMO and NMO were treated with a 1 M $HNO_3$ solution, 98% of the $Li^+$ and 85% of the $Na^+$ could be extracted from the solids, respectively. The Mn dissolutions were fairly low (5% for LMO and 2% for NMO). The Mn dissolution is due to a disproportionation reaction of Mn(III) (Mn(III) → $^1/_2$Mn(IV) + $^1/_2$Mn(II)) in the acid solution. The spinel structure of LMO and the birnessite structure of NMO remain after the acid treatment (Figure 4). This indicates that the $Li^+$ and $Na^+$ extraction reactions proceed topotactically, maintaining the spinel and birnessite structures, respectively. The lattice constant ($a_0$) of the spinel structure decreases slightly from 8.18 to 8.05 Å. On the other hand, the interlayer distance of the birnessite structure increases slightly from 7.19 to 7.25 Å.

The DTA-TG curves for LMO(H) showed endothermic peaks around 150 and 540 °C with weight losses, and an exothermic peak around 230 °C (Figure 3a). The DTA-TG curves are similar to those for the spinel-type manganese oxides prepared by solid state reaction.[18-20] The endothermic peak around 150 °C corresponds to the dissipation of water by the condensation of the lattice −OH group in the spinel structure, accompanied by a transformation of $H^+$-form spinel to $\beta$-$MnO_2$.[19,20] The exothermic peak around 230 °C corresponds to a transformation of $\lambda$-$MnO_2$ to $\beta$-$MnO_2$; $\lambda$-$MnO_2$ is formed by the redox-type extraction reaction of $Li^+$ from $LiMn_2O_4$ spinel.[18-20] The endothermic peak around 540 °C corresponds to a transformation of $\beta$-$MnO_2$ to $Mn_2O_3$ with a release of oxygen.[18-20]

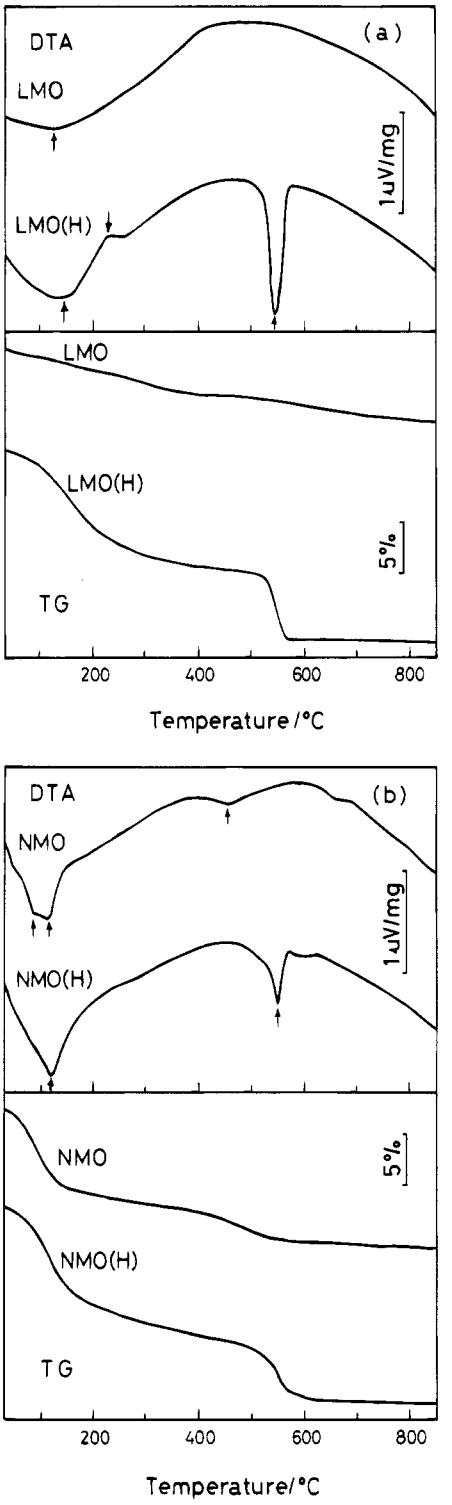


**Figure 3.** DTA (top) and TG (bottom) curves of the samples before and after acid treatment: (a) LMO and LMO(H); (b) NMO and NMO(H).

The DTA-TG curves for NMO(H) showed endothermic peaks around 120 and 550 °C with weight losses (Figure 3b). X-ray diffraction study indicated that the endothermic peak around 120 °C corresponds to a transformation of birnessite to $\gamma$-$MnO_2$, and the endothermic peak around 550 °C to a transformation of $\gamma$-$MnO_2$ to

(32) Rossouw, M. H.; Kock, A. D.; Picciotto, L. A. D.; Thackeray, M. M.; David, W. I. F.; Ibberson, R. M. *Mater. Res. Bull.* **1990**, *25*, 173.
(33) Kock, A. D.; Rossouw, M. H.; Picciotto, L. A. D.; Thackeray, M. M.; David, W. I. F.; Ibberson, R. M. *Mater. Res. Bull.* **1990**, *25*, 657.
(34) Burns, R. G.; Burns, V. M. *Manganese Dioxide Symposium*; Tokyo, 1980, p 97, Cleveland, Ohio; Vol. 2.
(35) Bach, S.; Pereira-Ramoss, J. P.; Baffier, N.; Messina, R. *Electrochim. Acta* **1991**, *36*, 1595.
(36) Goff, P. L.; Baffier, N.; Bach, S.; Pereira-Ramos, J. P.; Messina, R. *Solid State Ionics* **1993**, *61*, 309.

**Table 1. Composition of Starting, Prepared, and Acid-Treated Manganese Oxides**

| sample | $Z_{Mn}$[a] | M/Mn[b] | $H_2O$/Mn |
|---|---|---|---|
| $\gamma$-$MnO_2$ | 3.90 | | |
| LMO | 3.89 | 0.734 | 0.23 |
| NMO | 3.90 | 0.397 | 0.59 |
| LMO(H) | 4.00 | 0.01 | 0.60 |
| NMO(H) | 3.96 | 0.06 | 0.77 |

[a] $Z_{Mn}$: mean oxidation number of manganese. [b] M: Li, Na.

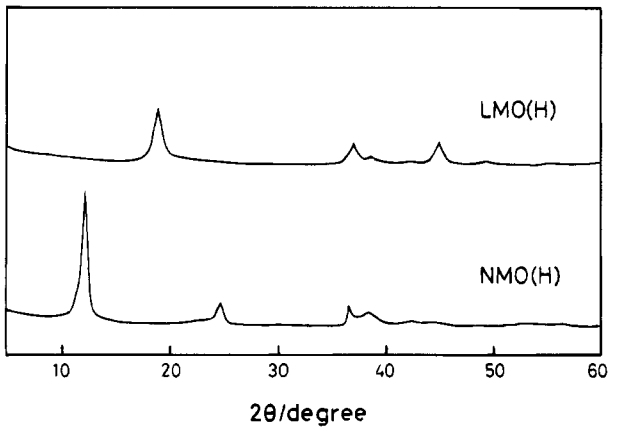


**Figure 4.** X-ray diffraction patterns of the acid-treated samples.

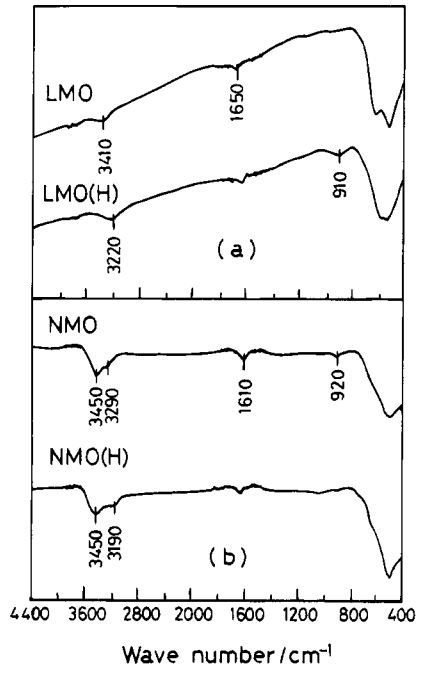


**Figure 5.** IR spectra of the samples before and after acid treatment: (a) LMO and LMO(H); (b) NMO and NMO(H).

$Mn_2O_3$ with a release of oxygen. The peak around 120 °C can be attributed to the dehydration of the crystal water in the birnessite structure as well as dissipation of water by the condensation of the lattice −OH group in the crystal, accompanying the formation of $\gamma$-$MnO_2$.

IR spectra of LMO, LMO(H), NMO, and NMO(H) are shown in Figure 5. In the spectrum of LMO (Figure 5a), the absorption bands at 3410 and 1650 $cm^{-1}$ can be assigned to stretching and bending vibrations of adsorbed water, respectively. The bands in the region from 400 to 750 $cm^{-1}$ can be assigned to Mn−O stretching vibrations.[11,20] In the spectrum of LMO(H), the absorption bands at 3220 and 910 $cm^{-1}$ can be assigned to stretching vibration of the lattice −OH group and lattice coupling vibration of the $H^+$-form spinel.[11,20] These facts indicate that some $Li^+$ are extracted from LMO by $Li^+/H^+$ ion-exchange reaction.

In the spectrum of NMO (Figure 5b), the bands at 3450 and 3290 $cm^{-1}$ can be assigned to stretching vibrations of the −OH group of adsorbed and molecules of the water of crystallization, respectively. The band at 3290 $cm^{-1}$ shifts to 3190 $cm^{-1}$ after acid treatment. The band at 3190 $cm^{-1}$ can be assigned to stretching vibration of the lattice −OH group or $H_3O^+$ in the crystal. This suggests that $Na^+/H^+$ ion-exchange reaction occurs in the $Na^+$ extraction process.

The results of compositional analysis for acid-treated samples are shown in Table 1. The water content ($H_2O$/Mn mole ratio) increase in the acid-treated samples, owing to the $Li^+/H^+$ or $Na^+/H^+$ ion-exchange reactions. The increases of the mean oxidation number ($Z_{Mn}$) in the acid-treated samples are due to a disproportionation reaction of Mn(III) to Mn(IV) and Mn(II) in the extraction processes. Studies on the extraction of alkali-metal ions from spinel-type and hollandite-type manganese oxides indicated that the disproportionation of Mn(III) is responsible for the redox-type extraction reaction.[19,20,26,27]

**Extraction Reactions.** On the basis of the previous studies on the spinel- and hollandite-type manganese oxides,[19,20,26,27] it is reasonable to consider that both ion-exchange-type and the redox-type reactions generally occur in the alkali-metal ion extraction from manganese oxides. The ion-exchange-type reaction can be described simply as

$$(A)Mn(IV) + H^+ \rightarrow (H)Mn(IV) + A^+ \quad (1)$$

and the redox-type reaction which is a disproportionation reaction of Mn(III) in acidic solution can be described as

$$(A)Mn(III) \rightarrow {}^1/_2(A)Mn(IV) + A^+ + {}^1/_2Mn^{2+} \quad (2)$$

where (A)Mn(IV) and (A)Mn(III) denote ion-exchange-type and redox-type sites in the solid phase, respectively, and $A^+$ alkali-metal ion. All manganese ions responsible for ion-exchange reactions are in the tetravalent state. The trivalent manganese is related to the redox-type site. The extraction of one alkali-metal ion from the redox-type site accompanies the disproportionation of one Mn(III) to Mn(IV) and Mn(II) at the crystallite surface.

On the basis of reactions 1 and 2, the extraction reaction for LMO can be described as

$$Li_{1.27}Mn(III)_{0.19}Mn(IV)_{1.54}O_4 + 1.46H^+ \rightarrow 0.945H_{0.108}Mn(IV)_{1.73}O_4 + 1.27Li^+ + 0.095Mn^{2+} + 0.22H_2O \quad (3)$$

This equation shows that 85% and 15% of $Li^+$ are extracted by the $Li^+/H^+$ ion-exchange-type reaction and the redox-type reaction, respectively. The extraction reaction for NMO can be written as

$$Na_{0.40}Mn(III)_{0.10}Mn(IV)_{0.90}O_{2.15} + 0.40H^+ \rightarrow 0.97H_{0.28}Na_{0.06}Mn(IV)O_{2.15} + 0.34Na^+ + 0.030Mn^{2+} + 0.065H_2O \quad (4)$$

where 82% and 18% of $Na^+$ are extracted by the $Na^+/H^+$ ion-exchange-type reaction and the redox-type reaction, respectively. Equations 3 and 4 suggest that the $Li^+$ or $Na^+$ are extracted mainly by the ion-exchange reaction.

**pH Titration.** The pH titration curves of the acid-treated samples LMO(H) and NMO(H) in (0.1 M ACl + AOH, A = Li, Na, K, and Cs) solutions are shown in Figure 6. The LMO(H) shows an alkali-metal ion adsorptive property (Figure 6a) similar to the spinel prepared by the solid-state reaction of $Li_2CO_3$ with $MnCO_3$ at 400 °C.[20] This suggests that a similar material can also be obtained at a low temperature by hydrothermal reaction. LMO(H) has a remarkably larger apparent adsorptive capacity for $Li^+$ than $Na^+$ and $K^+$ over the pH range studied. This indicates that LMO(H) showed a lithium-ion-sieve property; $Li^+$ with a small ionic radius can enter the three-dimensional (1 × 3) tunnel of the spinel structure, while $Na^+$ and $K^+$ with larger ionic radii cannot do that but can only be adsorbed on the sites of the crystal surface which are nonspecific for metal ions.[19,20] The dibasic acid behavior toward $Li^+$ indicates that there are two types of adsorptive sites for $Li^+$. One is an ion-exchange-type, and the other is a redox-type. The formations of a small amount of $O_2$ gas and Mn(VII) were observed in the $Li^+$ titration system when the pH value of solution was higher than 6. This suggests that a stronger acidic site, dissociating below pH 5, can be ascribed to the ion-exchange-type site, and a weaker acidic site, dissociating above pH 5, can be ascribed to the redox-type site. The insertion of $Li^+$ into the redox-type sites accompanies reduction of Mn(IV) to Mn(III) as well as an evolution of oxygen gas (or a disproportionation of Mn(IV) to Mn(III) and Mn(VII) at the crystallite surface).[18-20,37]

NMO(H) showed monobasic acid behavior toward $Na^+$, $K^+$, and $Cs^+$, and tetrabasic acid behavior toward $Li^+$ (Figure 6b). This is different from the layered manganic acid[25] with an interlayer distance of 0.742 Å, which shows monobasic acid behavior toward $Na^+$, $K^+$, and $Cs^+$ but dibasic acid behavior toward $Li^+$. The apparent capacity of NMO(H) for the alkali-metal ion increases in the order $Li^+ < Na^+ \approx Cs^+ < K^+$ in the range of pH < 4. The capacity sequence changes to $Cs^+ < K^+ < Na^+ < Li^+$ in the range of pH > 10; the sequence is in agreement with the decreasing order of the effective ionic radii of metal ions, showing a steric effect in a state of high metal ion loading. Similar to the $Li^+$–spinel titration system, the evolution of a small amount of $O_2$ gas and the formation of Mn(VII) were also observed in the $Li^+$–NMO(H) titration system when the pH value was higher than 11. This indicates that a small amount of $Li^+$ can be inserted into the NMO(H) by the redox-type reaction. The insertion of $Li^+$ above pH 11 may be due to the redox-type reaction.

**Characterization of Metal-Ion-Loaded Samples.** Structural and compositional studies were carried out on the $Li^+$-loaded spinel, and the $Li^+$- and $K^+$-loaded birnessites. The spinel and birnessite structures remained after the metal ion loading. This indicates that the metal ion insertion reactions proceed topotactically. The lattice constant ($a_0$) of the spinel slightly increases with the $Li^+$ insertion.

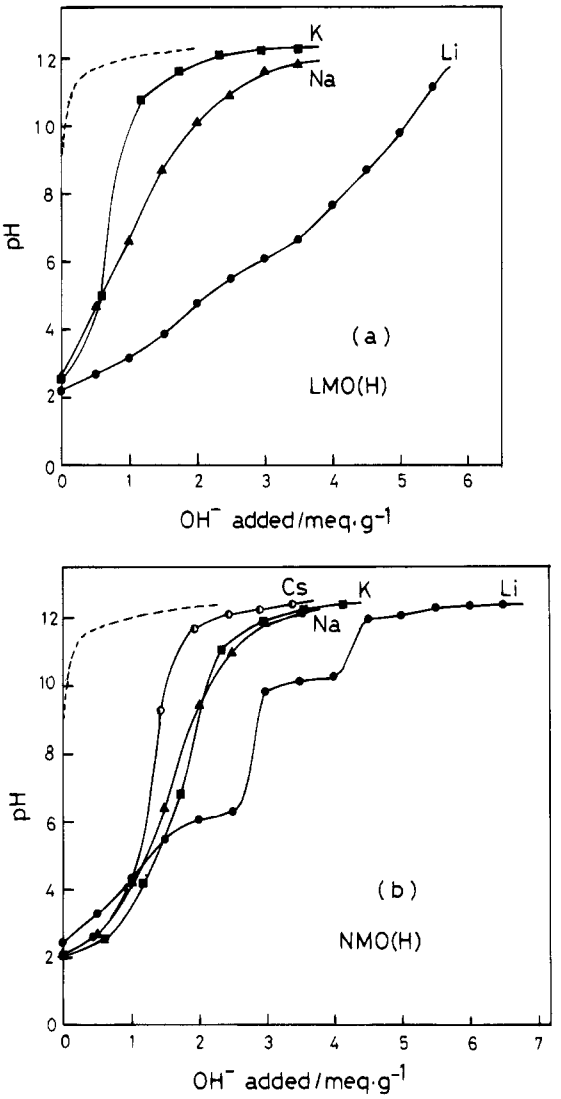


**Figure 6.** pH titration curves of acid-treated samples: (a) LMO(H), and (b) NMO(H). Sample, 0.1 g; solution, 0.1 M ACl + AOH (A = Li (●), Na (▲), K (●), or Cs (○)); total volume of solution, 10 mL; temperature, 20 °C; (- - -) blank titration.

The interlayer distance of the birnessite and the pH value of the titration solution are shown as a function of $Li^+$ and $K^+$ contents in Figure 7. The decreases in the interlayer distance may be due to an increase in the electrostatic attraction between the inserted metal ions and the sheets of edge-shared $MnO_6$ octahedra. The slight increase in the interlayer distance for the $Li^+$-loaded birnessite in the range of Li/Mn > 0.23 may be due to the reduction of Mn(IV) to Mn(III) by $Li^+$ insertion. The interlayer distance for the $K^+$-loaded samples is in agreement with that for the corresponding $Li^+$-loaded samples in a range of M/Mn < 0.15. This suggests that alkali-metal ions occupy the same sites of the interlayer in this range and that these sites are nonspecific for the adsorption of alkali-metal ions. The sites in the range of M/Mn > 0.15 can be ascribed to be specific for $Li^+$.

The water content of the $Li^+$-loaded spinel and the $Li^+$- and $K^+$-loaded birnessites is plotted as a function

(37) Kanzaki, Y.; Taniguchi, A.; Abe, M. *J. Electrochem. Soc.* **1991**, *138*, 333.

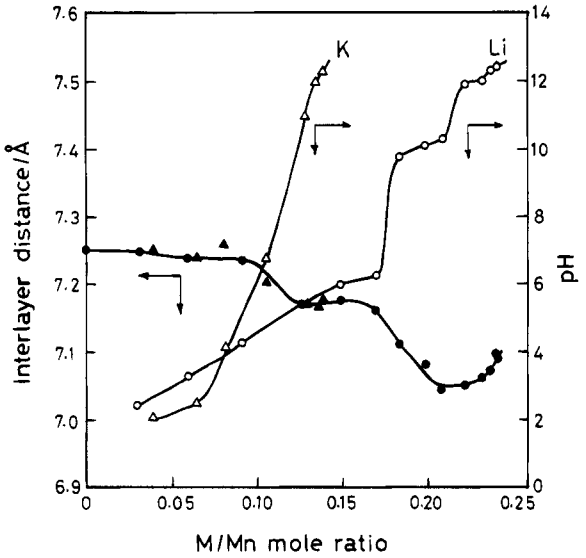


**Figure 7.** Interlayer distances (●, ▲) for the $Li^+$- and $K^+$-loaded birnessite-type manganese oxides and pH values (○, △) of the titration solutions as a function of $Li^+$ (●, ○) and $K^+$ (▲, △) contents.

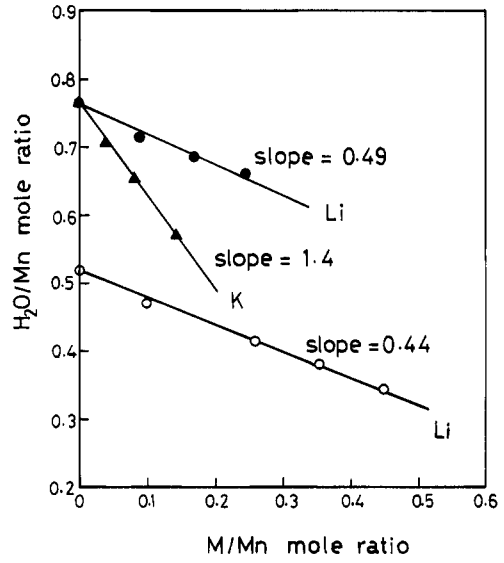


**Figure 8.** Water content of $Li^+$-loaded spinel-type manganese oxide (○) and $Li^+$- and $K^+$-loaded birnessite-type manganese oxides (●, ▲) as a function of $Li^+$ and $K^+$ contents.

of the metal ion content in Figure 8. The water content of both spinel and birnessite samples decreases linearly with an increase in the alkali-metal ion content. The decrease of the water content is due to the $H^+/Li^+$ or $H^+/K^+$ ion-exchange-type insertion reaction. In the $Li^+$−spinel system, the slope (0.44) is slightly smaller than the expected value (0.5) of the idealized ion-exchange reaction, probably owing to the presence of a small amount of redox-type insertion reaction. The slope (0.49) in the $Li^+$−birnessite system is close to the expected value of 0.5. This suggests that $Li^+$ insertion proceeds mostly by a stoichiometric $H^+/Li^+$ ion-exchange-type reaction. The higher slope (1.4) than 0.5 for $K^+$-loaded birnessite suggests that the insertion of $K^+$ accompanies a dehydration of the birnessite.

**Model for the Alkali-Metal Ion Insertion with Birnessite.** Several structural studies on birnessite-type manganese oxides have indicated that there are the following two types of crystallographic sites for the metal ions.[28,31,34,35] Alkali-metal ions (such as $Na^+$, $K^+$, $Cs^+$) with large ionic radii locate on the sheet of water of crystallization (A site, Figure 9).[28,31] Transition-metal ions (such as $Zn^{2+}$, $Cu^{2+}$, $Ni^{2+}$) with small ionic radii locate between the sheet of the edge-shared $MnO_6$ octahedra and the sheet of water of crystallization (B site, Figure 9), and adjacent to the manganese vacancies.[34,35] We suppose that the alkali-metal ions (such as $Na^+$, $K^+$, $Rb^+$, and $Cs^+$) with large ionic radii are inserted into the A sites. $Li^+$ can be inserted into the A sites the same as other alkali metal ions in the range of Li/Mn < 0.15. Since $Li^+$ have a small ionic radius, they can shift from the A sites to the B sites in the range of Li/Mn > 0.15. Dehydration of the birnessite by the $K^+$ insertion can be explained on the basis that $K^+$ has a large ionic radius and occupies the A site (the site of water of crystallization). The insertion of the metal ion into the B site will not be accompanied with the dehydration of the birnessite.

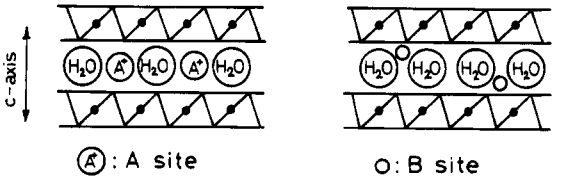


**Figure 9.** Structural model for the alkali-metal ion insertion into the birnessite-type manganese oxide: projection along *b* axis, omission of the manganese vacancies in $MnO_6$ octahedral sites.

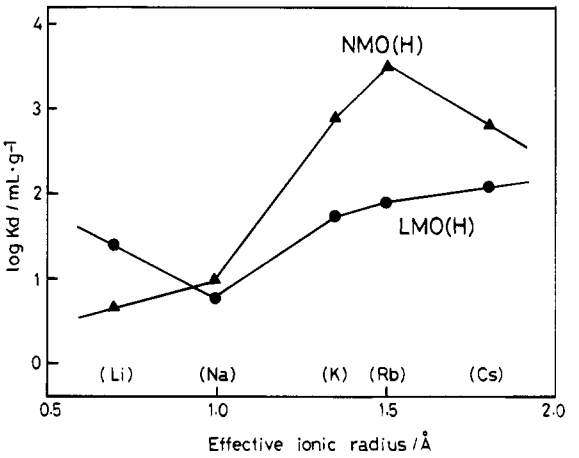


**Figure 10.** Distribution coefficients of alkali metal ions on LMO(H) (●) and NMO(H) (▲) at pH 2 as a function of effective ionic radius.

**Selectivity of Alkali-Metal Ions.** The equilibrium Kd values of alkali-metal ions of acid-treated samples LMO(H) and NMO(H) were measured at pH 2. A plot of log $K_d$ against the effective ionic radius of the metal ions[38] is shown in Figure 10. LMO(H) showed a selectivity sequence of $Na^+ < Li^+ < K^+ < Rb^+ < Cs^+$ for alkali-metal ions. The relatively high selectivity for $Li^+$ can be explained by the ion-sieve effect of the spinel lattice which has a three-dimensional (1 × 3) tunnel suitable in size for fixing lithium ions, similar to the cases of the manganese oxides prepared by solid-state reaction.[10-22] Namely, lithium ions can enter the (1 × 3) tunnel after dehydration, while other metal ions cannot do that, because their ionic radii are too large. These ions exchange with surface protons alone in

(38) Shannon, R. D.; Prewitt, C. T. *Acta Crystallogr.* **1969**, *B25*, 925.

hydrated forms, which gives a selectivity sequence which increases with the decrease in the radius of hydrated ion.

NMO(H) showed a selectivity sequence of $Li^+ < Na^+ < Cs^+ \approx K^+ < Rb^+$ for alkali-metal ions. A characteristic feature is that NMO(H) showed the highest selectivity for the adsorption of $Rb^+$ with an effective ionic radius around 1.5 Å (Figure 10). This is due to the ion-sieve effect of the birnessite lattice. The birnessite lattice is suitable in size for fixing an ion with an effective ionic radius of about 1.5 Å. In other words, the metal ions having almost same size as adsorptive sites in the interlayer spacing are strongly held by NMO(H), while the larger cations than the adsorptive sites suffer steric hindrance and the smaller cations are loosely bound by the weaker electrostatic attraction force. A similar metal ion adsorptive behavior was observed also for hollandite- or cryptomelane-type manganese oxides which have a one-dimensional (2 × 2) tunnel structure and show highest selectivity for the adsorption of metal ions with an effective ionic radius around 1.4 Å.[23,26]

It can be said that LMO(H) and NMO(H) have effective pore radii of about 0.7 and 1.5 Å for the adsorption of the metal ions, respectively.

## Conclusions

The spinel-type lithium manganese oxide and the birnessite-type sodium manganese oxide can be prepared by hydrothermal treatment of $\gamma$-$MnO_2$ with LiOH and NaOH solutions, respectively. $Li^+$ and $Na^+$ can be topotactically extracted from the lithium manganese oxide and the sodium manganese oxide by acid treatment, respectively. The acid-treated samples show ion-sieve properties for the adsorption of metal ions. The effective pore radii of LMO(H) and NMO(H) are about 0.7 and 1.5 Å, respectively.

CM9500162